

# OctFormer: Octree-based Transformers for 3D Point Clouds

PENG-SHUAI WANG, Peking University, China

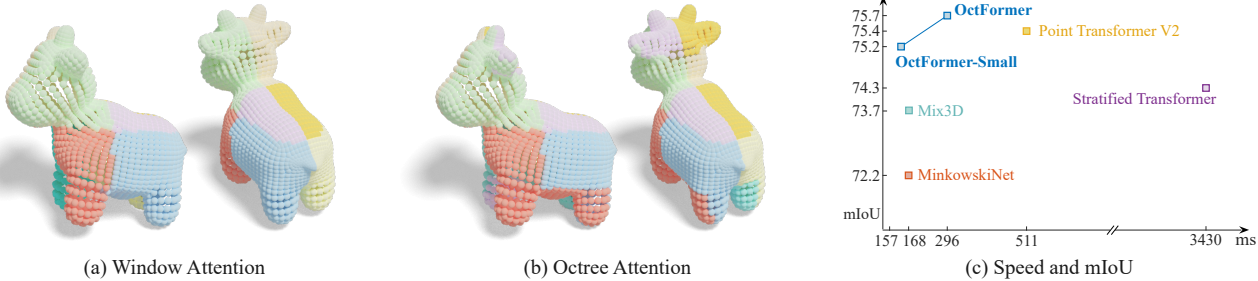


Fig. 1. Octree Attention and the superiority of OctFormer. (a): The window attention partitions the point cloud with cubic windows and constrains the attention in each window to accelerate the global attention. Each window is encoded by a specific color, as indicated by the front and back view of the point cloud. The point number in each window is highly unbalanced, which incurs great computation cost. (b): Our octree attention partitions the point cloud according to the sorted shuffled keys of the octree, ensuring an equal number of points in each window. (c): OctFormer built upon our octree attention achieves the best mIoU and efficiency on ScanNet compared with representative sparse-voxel-based CNNs and point cloud transformers. The horizontal axis represents the time of one forward pass of each network on an Nvidia 3090 GPU, taking a batch of 250k points.

We propose octree-based transformers, named OctFormer, for 3D point cloud learning. OctFormer can not only serve as a general and effective backbone for 3D point cloud segmentation and object detection but also have linear complexity and is scalable for large-scale point clouds. The key challenge in applying transformers to point clouds is reducing the quadratic, thus overwhelming, computation complexity of attentions. To combat this issue, several works divide point clouds into non-overlapping windows and constrain attentions in each local window. However, the point number in each window varies greatly, impeding the efficient execution on GPU. Observing that attentions are robust to the shapes of local windows, we propose a novel octree attention, which leverages sorted shuffled keys of octrees to partition point clouds into local windows containing a fixed number of points while permitting shapes of windows to change freely. And we also introduce dilated octree attention to expand the receptive field further. Our octree attention can be implemented in 10 lines of code with open-sourced libraries and runs 17 times faster than other point cloud attentions when the point number exceeds 200k. Built upon the octree attention, OctFormer can be easily scaled up and achieves state-of-the-art performances on a series of 3D segmentation and detection benchmarks, surpassing previous sparse-voxel-based CNNs and point cloud transformers in terms of both efficiency and effectiveness. Notably, on the challenging ScanNet200 dataset, OctFormer outperforms sparse-voxel-based CNNs by 7.3 in mIoU. *Our code and trained models are available at <https://wang-ps.github.io/octformer>.*

CCS Concepts: • Computing methodologies → Shape analysis; Point-based models; Neural networks.

Additional Key Words and Phrases: Point Clouds, Transformers, Octree, 3D Semantic Segmentation, 3D Object Detection

Author's address: Peng-Shuai Wang, Peking University, China, wangps@hotmail.com.

© 2023 Copyright held by the owner/author(s). Publication rights licensed to ACM. This is the author's version of the work. It is posted here for your personal use. Not for redistribution. The definitive Version of Record was published in *ACM Transactions on Graphics*, <https://doi.org/10.1145/3592131>.

## ACM Reference Format:

Peng-Shuai Wang. 2023. OctFormer: Octree-based Transformers for 3D Point Clouds. *ACM Trans. Graph.* 42, 4 (August 2023), 11 pages. <https://doi.org/10.1145/3592131>

## 1 INTRODUCTION

3D point cloud understanding is a fundamental task in computer graphics and vision and has a broad range of applications, including robotics, autonomous driving, and augmented reality. A variety of deep learning methods have been proposed for it, such as voxel-based CNNs [Graham et al. 2018; Wang et al. 2017; Wu et al. 2015], view-based CNNs [Su et al. 2015], and point-based networks [Li et al. 2018; Qi et al. 2016, 2017b], and remarkable progress has been made. Recently, point cloud transformers have emerged [Guo et al. 2021; Misra et al. 2021; Zhao et al. 2021] as an effective alternative with the potential for cross-multimodality training and general intelligent models [Radford et al. 2021; Ramesh et al. 2022].

However, the efficiency of point cloud transformers is still much worse than their CNN counterparts [Choy et al. 2019; Nekrasov et al. 2021; Wang et al. 2017], especially on scene-scale datasets like ScanNet [Dai et al. 2017], and the performance of point cloud transformers is also just comparable. Since it has been proven that transformers are at least as expressive as CNNs [Cordonnier et al. 2020], one of the key challenges of applying transformers to point clouds is to overcome the huge computational complexity of transformers, which is quadratic with the number of elements involved. Several methods [Guo et al. 2021; Pang et al. 2022; Yu et al. 2022] directly apply transformers to all points globally, thus limiting their applicability to large-scale point clouds. Following the progress in scaling up vision transformers [Dong et al. 2022; Liu et al. 2021a], one effective strategy is to constrain point cloud transformers within non-overlapping local windows [Fan et al. 2022; Lai et al. 2022; Mao et al. 2021; Sun et al. 2022]. However, unlike images, the number of points across different local windows varies significantly due to

the sparsity of point clouds. To deal with this issue, sophisticated implementations like region batching [Fan et al. 2022; Sun et al. 2022] or customized GPU kernels [Lai et al. 2022] have to be adopted, which severely impedes massive parallelism on GPUs. Another strategy to speed up point cloud transformers is to apply transformers in downsampled feature maps [Cheng et al. 2021b; Park et al. 2022], which also weakens the network capability and incurs a decrease in performance.

In this paper, we present a general and scalable octree-based transformer, abbreviated as OctFormer, for learning on 3D point clouds. The key building block of OctFormer is a novel octree attention mechanism for point clouds. To retain linear complexity, we divide each point cloud into small groups when applying attentions. Our key observation is that attentions are insensitive to the actual shape of underlying local windows. Instead of using cubic windows as in previous works, which incur variant point numbers in each window, we divide point clouds into groups with irregular windows while keeping the point number in each window the same. Consequently, we can easily implement our attention using standard operators provided by deep learning frameworks like PyTorch [Paszke et al. 2019]. To generate the required window partition, our second observation is that after constructing an octree with the parallel algorithm in [Zhou et al. 2011], the octree nodes are sorted in z-order by shuffled keys [Wilhelms and Van Gelder 1992], which ensures that spatially-close octree nodes are contiguously stored in memory. We store features in tensors according to the order of octree nodes. After padding a few zeros to make the spatial numbers of tensors divisible by the specified point number in each window, we can efficiently generate the window partition by simply reshaping the tensors at almost zero cost. An example is shown in Figure 1-(b), where the point number in each window is the same. To further increase the receptive fields of OctFormer, we introduce a dilated octree attention with dilated partitions along the spatial dimension of tensors, which can also be efficiently implemented with tensor reshaping and transposing.

Our OctFormer challenges conventional wisdom in designing point cloud transformers from two aspects. First, instead of using fixed-sized local windows, we fix the point number in each window when doing point cloud partition, enabling simple implementation and easy parallelization; second, instead of regarding point clouds as unordered and unstructured point sets, we actually sort the quantized points with shuffled keys by building octrees, resulting in a convenient window partition. Our octree attention completely eliminates the expensive neighborhood searching used in previous designs [Lai et al. 2022; Wu et al. 2022], bypasses the sparsity of point clouds, and can be reduced to a standard multi-head self-attention [Vaswani et al. 2017] on small groups of equal size. Consequently, our octree attention can be implemented in *10 lines of code* with open-sourced libraries freely available on the web. One *single* transformer block on top of octree attention runs at least *17 times faster* than previous state-of-the-art point transformer blocks [Lai et al. 2022; Wu et al. 2022] when the number of elements involved is 200k.

We also introduce feature hierarchies following the multiscale structure of octrees, endowing OctFormer with the capability as a general backbone for 3D segmentation and detection. We verify the effectiveness of OctFormer on a series of 3D benchmarks. Specifically, our OctFormer achieves the best performance on the validation

set of ScanNet segmentation [Dai et al. 2017], SUN RGB-D detection [Song et al. 2015], and ScanNet200 segmentation [Rozenberszki et al. 2022], surpassing all previous state-of-the-art sparse-voxel-based CNNs [Choy et al. 2019; Graham et al. 2018; Wang et al. 2017] and point cloud transformers [Lai et al. 2022; Wu et al. 2022] by a large margin. Notably, on ScanNet200 segmentation, which contains 200 semantic categories (ten times more than ScanNet), the mIoU of our OctFormer is higher than MinkowskiNet [Choy et al. 2019] by 7.3 and even higher than the recently-proposed LGround [Rozenberszki et al. 2022] by 5.4, which pretrains a sparse-voxel-based CNN with a powerful CLIP model [Radford et al. 2021].

In summary, our main contributions are as follows:

- We propose a novel octree attention and its dilated variant, which are easy to implement and significantly more efficient than previous point cloud attentions;
- We propose OctFormer, which can serve as a general backbone for 3D point cloud segmentation, detection, and classification;
- OctFormer achieves state-of-the-art performances on a series of 3D segmentation and detection benchmarks, and the computational efficiency of OctFormer is much higher than previous point cloud transformers and even surpasses highly optimized sparse-voxel-based CNNs.

## 2 RELATED WORK

*Voxel-based CNNs.* Full-voxel-based CNNs generalize 2D CNNs to 3D learning by representing 3D data with uniformly-sampled voxels [Maturana and Scherer 2015; Qi et al. 2016; Wu et al. 2015]. However, these methods can only take low-resolution voxels like  $32^3$  as input due to their cubic computational and memory cost with regard to the voxel resolution. Sparse-voxel-based CNNs greatly improve the efficiency of full-voxel-based CNNs by constraining CNN operations into non-empty sparse voxels and adopting octrees [Wang et al. 2017, 2018] or hash tables [Choy et al. 2019; Graham et al. 2018; Shao et al. 2018] to facilitate neighborhood searching for convolutions. Several other networks also leverage octrees [Lei et al. 2019; Riegler et al. 2017b,a] for improving the efficiency of full-voxel-based CNNs. Sparse-voxel-based CNNs mainly use small convolution kernels, while it has been proven that large convolution kernels can greatly improve network performance [Chen et al. 2022] in practice. Our OctFormer can easily enlarge its window size and has a much larger receptive field than sparse-voxel-based CNNs.

*Point-based Networks.* Instead of rasterizing 3D shapes into regular voxels, point-based networks directly take raw point clouds as input. Since point clouds are unordered and unstructured, these networks employ permutation-invariant operations [Li et al. 2018; Qi et al. 2017a,b], continuous convolution kernels [Atzmon et al. 2018; Fey et al. 2018; Thomas et al. 2019], or adaptive weights [Simonovsky and Komodakis 2017; Wu et al. 2019] to aggregate and update point features. To query neighboring points, point-based networks construct a k-nearest-neighbor graph from input point clouds [Fey et al. 2018; Li et al. 2018; Qi et al. 2017b; Simonovsky and Komodakis 2017; Xu et al. 2018]. In order to extract hierarchical features, point-based networks often rely on farthest point sampling [Qi et al. 2017b] or grid-based sampling [Hu et al. 2020a;

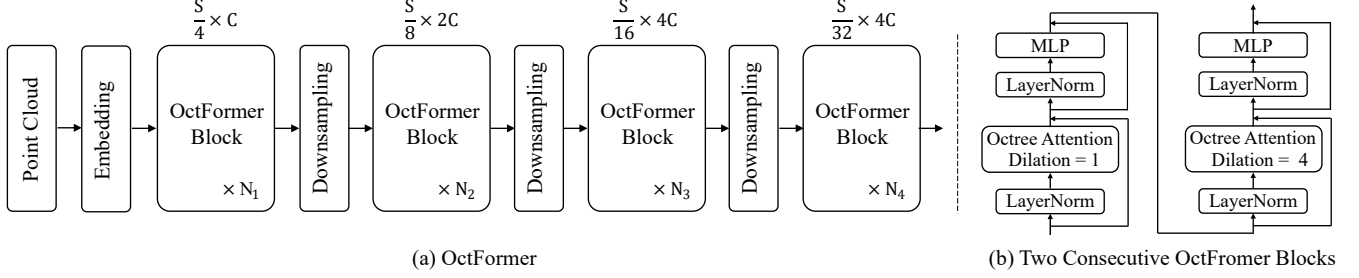


Fig. 2. Overview. (a): The architecture of OctFormer. OctFormer consists of an Embedding module, a sequence of OctFormer blocks and downsampling modules.  $S$  and  $C$  denote the spatial resolution and channel of features,  $N_i$  denotes the number of the corresponding OctFormer blocks. (b): Two consecutive OctFormer blocks. Each OctFormer block consists of an octree attention, an MLP, and two Layer Normalizations (LayerNorm). Two consecutive OctFormer blocks use dilations of 1 and 4 for their respective octree attentions.

Thomas et al. 2019] to downsample point clouds progressively. Our OctFormer also takes point cloud as input, but our novel octree attention totally avoids expensive k-nearest-neighbour search and farthest point sampling. As a result, OctFormer is much more efficient and outperforms previous point-based networks.

**Vision Transformers.** Inspired by the great success of transformers in natural language processing [Vaswani et al. 2017], ViT [Dosovitskiy et al. 2021] uses transformer-based networks for visual recognition. ViT partitions the input image into non-overlapping regular patches, considers each patch as a token, and applies pure attentions to these tokens. To extend ViT for dense prediction tasks such as image segmentation and detection, PVT [Wang et al. 2021] and Swin Transformer [Liu et al. 2021a] introduce hierarchical network architectures from CNNs to vision transformers. PVT proposes applying attention modules on downsampled feature maps to improve the efficiency of ViT when dealing with large images. On the other hand, Swin Transformer introduces shifted-window attentions to restrict attentions in non-overlapping local windows. Many follow-up works [Chu et al. 2021a; Dong et al. 2022; Wang et al. 2022b; Yang et al. 2021] further improve the attention designs with a similar network architecture. OctFormer also has a hierarchical network architecture. Our key innovation is a novel octree attention mechanism for point clouds, which utilizes variant local window shapes while maintaining a fixed number of points in each window for efficiency.

**Point Cloud Transformers.** Following vision transformers, it is natural to explore the extension of transformers for point cloud understanding. Point Cloud Transformer (PCT) [Guo et al. 2021] applies offset attentions to all point features for point cloud classification and segmentation. Point-BERT [Yu et al. 2022] and Point-MAE [Pang et al. 2022] utilize standard transformers trained on point clouds for unsupervised pre-training. 3DETR [Misra et al. 2021] proposes an end-to-end scheme for point cloud detection with standard transformers. However, these methods are limited to point clouds containing only a few thousand points due to the high computation and memory costs incurred by global attentions.

Point Transformer (PT) [Zhao et al. 2021] applies vector attentions to a local neighborhood of each point. Although PT has lower memory costs than PCT, its computation cost is still high due to the usage of expensive farthest point sampling when doing pooling operations

to downsample feature maps. Point Transformer V2 (PTv2) [Wu et al. 2022] enhances PT’s efficiency by substituting farthest point sampling with grid-based sampling and improves its performance further by utilizing grouped vector attentions and additional positional encoding multipliers. The attention modules of both PT and PTv2 are applied independently to local neighborhoods of each point in a sliding window fashion. Since there is no computation sharing among overlapping neighborhoods, significant computation resources are wasted.

To scale up point cloud transformers, SST [Fan et al. 2022], SWFormer [Sun et al. 2022], and Stratified Transformer [Lai et al. 2022] extend Swin Transformer [Liu et al. 2021a] for image understanding to point clouds by restricting attention modules to non-overlapping windows of point clouds. Since the number of points in each local window differs greatly, SST and SWFormer group local windows with similar numbers of points together and process them in batch mode; while Stratified Transformer leverages sophisticated GPU programs to combat this issue. Similar to the scaling strategy of PVT [Wang et al. 2021], PatchFormer [Cheng et al. 2021b] applies attention modules to patch features instead of point features; Fast Point Transformer [Park et al. 2022] downsamples the point cloud into low-resolution voxels and restricts the attention modules to those voxels. However, the performance of PatchFormer and Fast Point Transformer is worse than other contemporary point cloud transformers. Unlike previous point cloud transformers, our OctFormer divides the input point clouds into groups containing an equal number of points, making it easy to parallelize and scale up. Our OctFormer also achieves state-of-the-art performance on semantic segmentation and object detection on large-scale benchmarks.

### 3 OCTREE-BASED TRANSFORMERS

**Overview.** The overview of OctFormer is shown in Figure 2. Given an input point cloud, we first normalize it with a specified scale factor and convert it to an octree. The initial features include average point positions, colors, and point normals (if provided) stored in non-empty octree leaf nodes. Then an embedding module is used to downsample and project the initial features into a high-dimensional space. Next, a sequence of OctFormer blocks and downsampling modules are alternately applied to generate high-level hierarchical features, which can be consumed by a lightweight Feature Pyramid Network (FPN) [Kirillov et al. 2019; Lin et al. 2017] for semantic

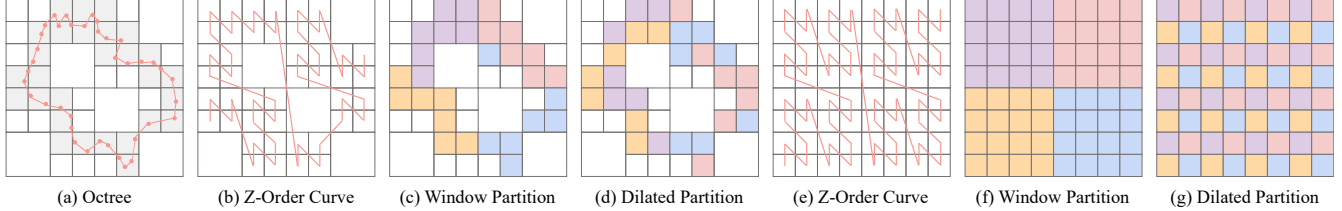


Fig. 3. Window partition for the octree attention. Here 2D images are shown for a better illustration. (a): An input point cloud sampled from a shape in red and the corresponding octree (quadtree). Non-empty octree nodes are highlighted in gray. (b): Z-order curve at depth 3 of the octree. (c): A window partition generated by tensor reshaping and transposing corresponding to (b), with a point number of 7. The features are stored in a tensor following the order of non-empty octree nodes on the z-order curve. (d): A dilated partition with a point number of 7 and a dilation of 2. (e): Z-order curve covering the whole space. (f): A window partition corresponding to (e) with a point number of 16. (g): A dilated partition corresponding to (e) with a point number of 16 and a dilation of 4.

segmentation and object detection. The core of OctFormer is a novel octree attention module as shown in Figure 2-(b), which is elaborated in Section 3.1. Other network components, including the embedding and downsampling module, the OctFormer block, and the detailed network configurations, are introduced in Section 3.2.

### 3.1 Octree Attention

*Attention.* Our octree attention is built upon the scaled dot-product attention proposed by [Vaswani et al. 2017], which is widely used in transformers in NLP and vision. We first review the attention module and introduce the observations motivating our octree attention. Denote an input feature map as  $X \in \mathbb{R}^{N \times C}$ , where  $N$  is the spatial number, and  $C$  is the channel number. Three learnable weight matrices  $W_q$ ,  $W_k$ , and  $W_v$  in  $\mathbb{R}^{C \times D}$  are used to map  $X$  to queries, keys and values. Then the attention can be defined as follows:

$$\text{Attention}(X) = \text{softmax}\left((XW_q)(XW_k)^T / \sqrt{D}\right)(XW_v). \quad (1)$$

Intuitively, the output can be regarded as a weighted sum of the values with weights dynamically computed from queries and the corresponding keys. The multi-head attention can be implemented by concatenating  $H$  independent attentions and merging the results with a linear layer, where  $H$  denotes the head number. In OctFormer, we adopt the multi-head attention by default, and we directly use the term attention to refer to the multi-head attention for simplicity.

According to Equation 1, the computation complexity of the attention is  $\mathcal{O}(N^2)$ , which is generally unaffordable when  $N$  exceeds several thousand, whereas point clouds from large-scale scanned datasets, such as ScanNet [Dai et al. 2017], often contain over 100k points. To scale up the attention, we leverage the strategy of window attentions [Liu et al. 2021a] to constrain the computation within non-overlapping local windows. Denote the point number in each local window as  $K$ , then the computation complexity of window attentions is reduced to  $\mathcal{O}(K^2 \cdot \frac{N}{K})$ , which is linear to  $N$ . A naive implementation is to follow vision transformers [Liu et al. 2021a] to partition point clouds into non-overlapping windows with 3D cubes [Fan et al. 2022; Lai et al. 2022; Sun et al. 2022]. However, different from images, the point number in each window varies greatly. Concretely, with a window size of 7 on ScanNet, the average point number is only 48, whereas the maximum point number is 343. This issue severely hampers the efficient execution of attentions on GPUs.

Observing that the attention aggregates features via weighted averages with weights normalized by a *softmax* function, we hypothesize that the attention is robust to the change of underlying window shapes. And we verify this observation empirically via a pilot study. Specifically, we use a ViT [Dosovitskiy et al. 2021] pretrained on a  $16 \times 16$  partition of images defined within a square window and alter the window shape by randomly masking out 20% of image patches, resulting in highly irregular windows. We utilize the codebase and weights provided by *timm* [Wightman 2019]. After the masking operation, the accuracy of ViT on the validation set of ImageNet [Deng et al. 2009] drops only slightly, from 85.1% to 84.2%. This observation motivates us to keep the point number in each local window constant while allowing the shape of local windows to vary freely, as opposed to simply using cubic windows. By keeping the point numbers fixed in every window, the parallelized computation of GPU can be fully exploited, and the implementation can be greatly simplified.

*Octree.* We adopt octrees to generate the required window partition and facilitate the hierarchical network architecture. For each point cloud, we employ the parallel algorithm proposed by [Zhou et al. 2011] to build an octree on GPU. After building the octree, octree nodes of the same depth are sorted with the shuffled keys [Wilhelms and Van Gelder 1992]. Denote the integer coordinates of an octree node as  $(x, y, z)$ , and the  $i^{th}$  bit of each coordinate as  $x_i$ ,  $y_i$ , and  $z_i$ , the shuffled key in binary expression is defined as follows:

$$\text{Key}(x, y, z) = x_1y_1z_1x_2y_2z_2 \dots x_dy_dz_d, \quad (2)$$

where  $d$  is the depth of the octree. The value of a shuffled key represents the position on the 3D z-order curve. We observe that octree nodes belong to one parent node, and more generally, octree nodes belonging to one subtree are contiguously stored in memory according to the z-order. This property of octrees is the key to our efficient window partition. A 2D illustration is shown in Figure 3. For an octree built from a point cloud marked in red color in Figure 3-(a), the corresponding z-order curve in depth 3 of the octree is shown in Figure 3-(b). Since the octree nodes are sparse, the full z-order curve is shown in Figure 3-(e) for reference.

*Octree Attention.* With sorted shuffled keys of octrees, we can easily generate window partitions through tensor reshaping and transposing. Note that only non-empty octree nodes contain feature vectors. We can trivially filter out empty nodes with the information

provided by octrees while preserving the original order. An example is shown in Figure 3-(a), where non-empty octree nodes are marked in gray color. We stack all features in non-empty octree nodes into a 2D tensor following the order of sorted shuffled keys. Denote the resulting feature tensor as  $X$  with a shape of  $(N, C)$ , we first pad zeros to create a new tensor  $\tilde{X}$  with a shape of  $(\tilde{N}, C)$ , so that  $\tilde{N}$  is divisible by the specified point number  $K$ , which is typically set to 32 in our experiments. Then we generate the window partition by reshaping  $\tilde{X}$  to  $(B, K, C)$ , where  $B$  equals  $\tilde{N}/K$  and denotes the total number of windows. With this partition, we can implement our octree attention by applying the attention in Equation 1 to these  $B$  windows in parallel while masking out the padded elements. An example is shown in Figure 3-(c), where  $K$  and  $N$  are equal to 7 and 28, respectively.

Although window attentions speed up the computation, they come with a reduced receptive field and a lack of information propagation among different windows. To alleviate these issues, we further propose a dilated octree attention. Denote the dilation as  $D$ , which is set to 1 or 4 in our experiments. For the octree attention described above, its dilation can be regarded as 1. When  $D$  is larger than 1, we pad  $X$  to  $\tilde{X}$  so that the spatial number  $\tilde{N}$  of  $\tilde{X}$  is divisible by  $K \times D$ . Next, we reshape  $\tilde{X}$  to a tensor with shape  $(\tilde{B}, K, D, C)$  where  $\tilde{B}$  equals  $\tilde{N}/(K \times D)$ . Then we transpose it to a tensor with shape  $(\tilde{B}, D, K, C)$ , and flatten the first two dimensions to get a tensor with shape  $(B, K, C)$ , with which the attention in Equation 1 can also be directly applied. An example is shown in Figure 3-(c), where  $K$  and  $D$  are equal to 7 and 2, respectively.

Albeit our octree attention is designed for sparse voxels, it degenerates to the standard window attention [Liu et al. 2021a] and dilated attention [Hassani and Shi 2022; Tu et al. 2022] in vision transformers when applied to full voxels or images with specific window size and dilation settings. An example is shown in Figure 3-(f)&(g), where the point number is 16, and the dilation is 4.

*Positional Encoding.* Positional encoding is essential for attentions to differentiate features defined at different positions. A widely-used strategy is to add relative positional bias [Liu et al. 2021a; Raffel et al. 2020] to the attention defined in Equation 1. Denote the maximum window size as  $W$ ; the relative positions of two arbitrary points within the same window lie in  $[-W + 1, W - 1]$ . Naively extending relative positional bias to 3D requires  $H \times (2W - 1)^3$  trainable parameters, where  $H$  is the head number of attention. With our octree attention, the maximum window size is at least 50 when the dilation is larger than 4, which greatly increases the parameters of our OctFormer. Therefore, we adopt the conditional positional encoding (CPE) [Chu et al. 2021b; Dong et al. 2022; Wang et al. 2022b], which dynamically generates the positional encoding conditioned on current features with a depthwise convolution. Specifically, we apply the octree-based depthwise convolution provided by O-CNN [Wang et al. 2017] and the Batch Normalization [Loffe and Szegedy 2015] to the input tensor  $X$  as positional encoding before each attention module:

$$X = X + \text{batch\_norm}(\text{depth\_wise\_conv}(X)) \quad (3)$$

With CPE, the network performance improves significantly while using fewer parameters than relative positional bias, as verified in our ablation study in Section 4.2.

---

**Algorithm 1** Pseudocode of Octree Attention in a PyTorch-like style.

---

```

# x: input tensor with a shape of (N, C)
# D: dilation for attention, set to 1 or 4 by default
# P: point number in each window, set to 32 by default
# attntion: an object of torch.nn.MultiheadAttention

# apply conditional positional encoding
x = x + batch_norm(depth_wise_conv(x))

# window partition
N, C = x.shape
Nz = (P * D) - N % (P * D) # number of zeros for padding
x = torch.cat([x, x.new_zeros(Nz, C)]) # pad zeros
x = x.reshape(-1, P, D, C).transpose(1, 2).flatten(0, 1)

# attention mask
m = torch.cat([x.new_zeros(N), x.new_ones(Nz)]).bool()
m = m.reshape(-1, P, D).transpose(1, 2).flatten(0, 1)

# apply attention
x = attntion(query=x, key=x, value=x, key_padding_mask=m)

# reverse window partition
x = x.reshape(-1, D, P, C).transpose(1, 2).reshape(-1, C)

output = x[:N] # remove the padded elements

```

---

*Summary.* Our octree attention is extremely easy to implement and much more efficient than previous point cloud attentions. With open-sourced libraries on the web, we can implement our octree attention in 10 lines of code when the batch size is 1, as summarized in Algorithm 1. The core of our octree attention can be implemented with the multi-head attention module provided by PyTorch – `torch.nn.MultiheadAttention` [Paszke et al. 2019], which is highly optimized based on general matrix multiplication routines on GPU. And tensor reshaping and transposing operators for window partition are also standard operators supported by PyTorch. The number of zeros for padding in our octree attention is  $(\tilde{N} - N)$ , which is less than  $K \times D$  (128 in our settings); thus the computation cost of padding is negligible. In contrast, the implementation of other point cloud attentions [Fan et al. 2022; Lai et al. 2022; Sun et al. 2022] requires complex engineering and customized GPU programming. We demonstrate the efficiency of our octree attention in Section 4.2.

### 3.2 Network Details

In this section, we introduce the remaining details of OctFormer, including the embedding module, the OctFormer block, and the downsampling module, as shown in Figure 2. Denote the initial spatial resolution of octree as  $S$ , the embedding module maps the input signal into a high-dimensional feature space and downsamples the spatial resolution by a factor of 4. Following the embedding module are four network stages, and each network stage is composed of  $N_i$  OctFormer blocks and a downsampling module, where  $i$  denotes the stage index. OctFormer blocks are used to process features; each downsampling module reduces the spatial resolution of features by a factor of 2 and increases the feature channel by a factor of 2 in each stage, except for the last stage, where the channel is kept as  $4C$  to reduce the total parameter number of the network.

*Embedding.* Instead of using a single convolution layer with a large kernel size and stride to instantiate the embedding module, as is

done in ViT [Dosovitskiy et al. 2021], we opt for several convolution layers with small kernel sizes, which has been shown to be able to stabilize the training process of transformers [Xiao et al. 2021]. In OctFormer, we use a series of 5 octree-based convolution modules for the embedding module. Each module consists of an octree convolution [Wang et al. 2017], a Batch Normalization layer [Loeffe and Szegedy 2015], and a ReLU activation function. The kernel sizes and strides of these octree convolutions are  $\{3, 2, 3, 2, 3\}$  and  $\{1, 2, 1, 2, 1\}$ , respectively. The convolutions with a stride of 2 downsample the spatial resolution of tensors by a factor of 2.

*OctFormer Block.* Following the standard transformer block design [Vaswani et al. 2017], an OctFormer block consists of an octree attention introduced in Section 3.1, a multilayer perceptron (MLP), and residual connections, as shown in Figure 2-(b). The MLP has two fully connected layers with a GELU activation function in between, and the expansion ratio of the hidden channel of MLP is set to 4. Layer Normalization (LayerNorm) [Ba et al. 2016] is employed prior to each attention module and each MLP to stabilize the training. The dilations of octree attention in two consecutive OctFormer blocks are set to 1 and 4, respectively.

*Downsampling.* The downsampling module is implemented as an octree convolution with a kernel size of 2 and a stride of 2, followed by a Batch Normalization layer, which reduces the spatial resolution and increases the channel of a feature map by a factor of 2.

*Network Settings.* By default,  $C$  is set to 96, the block numbers are set to  $\{2, 2, 18, 2\}$ , the head numbers of octree attentions are set to 1/16 of the channel numbers, and the point numbers for window partition are set to 32. The resulting OctFormer has a similar amount of trainable parameters (39M) as MinkowskiNet (38M) [Choy et al. 2019]. The output of OctFormer is hierarchical features with four spatial resolutions, i.e.,  $\{S/4, S/8, S/16, S/32\}$ , which can be conveniently integrated with a feature pyramid network (FPN) [Lin et al. 2017] for segmentation and detection. And the last feature map can be averaged as the global feature for shape classification.

## 4 EXPERIMENTS

In this section, we validate the effectiveness and efficiency of our OctFormer on 3D semantic segmentation and 3D object detection tasks. We also discuss our design choices in the ablation study. The experiments were conducted using 4 Nvidia 3090 GPUs with 24GB of memory.

### 4.1 3D Semantic Segmentation

We first verify the efficacy of our OctFormer on 3D semantic segmentation. The goal of this task is to predict the semantic label for each point in an input point cloud.

*Dataset.* The experiments are conducted on the ScanNet [Dai et al. 2017] dataset and the recently-proposed ScanNet200 [Rozenberszki et al. 2022] dataset. ScanNet contains 1513 large-scale 3D scans of indoor scenes and includes 20 semantic categories. The average point number of scans in ScanNet is 148k. ScanNet200 shares the same data as ScanNet, but has 200 semantic categories, making it more challenging. We follow the standard data splits [Dai et al. 2017]

Table 1. Semantic Segmentation on ScanNet. *Val.* and *Test* denote the mIoU on the validation and testing set, respectively. The best results are marked in bold. Our OctFormer achieves the best performance on the validation set, surpassing all point cloud transformers, sparse-voxel-based CNNs, and point-based networks. The mIoU of OctFormer without voting is shown in the parentheses for reference.

Method	Val.	Test
3DMV [Dai and Nießner 2018]	-	48.4
PanopticFusion [Narita et al. 2019]	-	52.9
PointNet++ [Qi et al. 2017b]	53.5	55.7
SegGCN [Lei et al. 2020]	-	58.9
JointPoint [Chiang et al. 2019]	69.2	63.4
RandLA-Net [Hu et al. 2020a]	-	64.5
PointConv [Wu et al. 2019]	61.0	66.6
PointASNL [Yan et al. 2020]	63.5	66.6
KPConv [Thomas et al. 2019]	69.2	68.6
FusionNet [Zhang et al. 2020a]	-	68.8
JSENNet [Hu et al. 2020b]	-	69.9
SparseConvNet [Graham et al. 2018]	69.3	72.5
MinkowskiNet [Choy et al. 2019]	72.2	73.6
LargeKernel [Chen et al. 2022]	73.2	73.9
O-CNN [Wang et al. 2017]	74.5	76.2
Mix3D [Nekrasov et al. 2021]	73.6	<b>78.2</b>
Point Transformer [Zhao et al. 2021]	70.6	-
Fast Point Transformer [Zhao et al. 2021]	72.1	-
Stratified Transformer [Lai et al. 2022]	74.3	73.7
Point Transformer V2 [Wu et al. 2022]	75.4	75.2
OctFormer (ours)	<b>75.7</b> (74.5)	76.6

for training and evaluation, using 1201 scans for training, 312 scans for validation, and 100 scans for testing. The testing labels are not publicly available, and testing results are obtained by submitting predictions to the official ScanNet website. We use the mean intersection over union (mIoU) over all categories as the evaluation metric.

*Settings.* OctFormer is used as the backbone to extract hierarchical features, and a lightweight FPN [Lin et al. 2017] is used as the segmentation head. The FPN first projects multiscale features with a convolution layer with a kernel size of 1 to make the channels of features equal to 168, then upsamples the features with the nearest interpolation by a factor of 2 and merges consecutive features by addition. The final output feature is processed by a convolution with a kernel size of 3 and upsampled to each point with the nearest neighbor interpolation, with which an MLP with one hidden layer is used to predict the point categories. For both ScanNet and ScanNet200, the training settings are the same, except that the output channel is 20 for ScanNet and 200 for ScanNet200. We employ an AdamW optimizer [Loshchilov and Hutter 2019] to train the network for 600 epochs with a batch size of 16 and a weight decay of 0.05. The initial learning rate is set as 0.006 and decreases by a factor of 10 after 360 and 480 epochs, respectively. The input point clouds are first normalized with a scale factor of 0.01m and then encoded by octrees with a depth of 11. The initial features include colors, normals, and point coordinates. The data augmentations include random rotation in  $[-180^\circ, 180^\circ]$ , random scaling in  $[0.75, 1.25]$ , random translation in  $[-0.1, 0.1]$ , random elastic deformations following [Choy et al. 2019], and random spherical cropping following [Lai et al. 2022].

Table 2. Semantic Segmentation on ScanNet200. *Head*, *Common* and *Tail* denote mIoUs on three smaller groups containing 66, 68 and 66 categories of ScanNet200, *All* denotes mIoU on all 200 categories. The best results are marked in bold. Our OctFormer trained from scratch achieves the best performance on all groups and are significantly better than previous state-of-the-art methods, even those with pretraining.

Method	Head	Common	Tail	All
CSC-Pretrain [Hou et al. 2021]	45.5	17.1	7.9	24.9
MinkowskiNet [Choy et al. 2019]	46.3	15.4	10.2	25.3
SupCon [Khosla et al. 2020]	48.6	19.2	10.3	26.0
LGround [Rozenberszki et al. 2022]	48.5	18.4	10.6	27.2
OctFormer (ours)	<b>53.9</b>	<b>26.5</b>	<b>13.1</b>	<b>32.6</b>

*Results on ScanNet.* We compare our OctFormer with a series of previous state-of-the-art methods on ScanNet and summarize the validation and testing mIoUs in Table 1. The training of our OctFormer takes 15 hours and consumes 13GB of memory using 4 Nvidia 3090 GPUs. Our OctFormer achieves a mIoU of 74.5 on the validation set without voting. Since Stratified Transformer [Lai et al. 2022] employs block-wise prediction and Point Transformer V2 [Wu et al. 2022] employs the voting strategy to improve the performance, we also adopt the voting strategy, which results in a mIoU of 75.7 as shown in Table 1. Clearly, our OctFormer achieves the best performance on the validation set among all methods. Specifically, OctFormer outperforms previous point cloud transformers with a validation mIoU higher than Stratified Transformer [Lai et al. 2022] by 1.4 and Point Transformer [Zhao et al. 2021] by 5.1. OctFormer also surpasses sparse-voxel-based CNNs with a validation mIoU higher than SparseConvNet [Graham et al. 2018] by 6.4, MinkowskiNet [Choy et al. 2019] by 3.5, and LargeKernel [Chen et al. 2022] by 2.5. Additionally, OctFormer significantly outperforms point-based networks, including PointNet++ [Qi et al. 2017b] and KPConv [Thomas et al. 2019]. On the testing set, our OctFormer achieves the second-best mIoU, as Mix3D currently ranks the first. However, our OctFormer achieves better mIoU than Mix3D on the validation set. One possible explanation is that Mix3D employs an additional mixup data augmentation and post-processing to further improve the testing results, as mentioned in [Nekrasov et al. 2021]. A visual comparison with Stratified Transformer is shown in Figure 5, which demonstrates that OctFormer can produce more faithful results in detailed regions.

*Results on ScanNet200.* Since object categories in ScanNet200 are highly imbalanced, the 200 categories of ScanNet200 are further split into three smaller groups of 66, 68 and 66 categories [Rozenberszki et al. 2022] according to the label frequency in the training set, which are denoted as Head, Common and Tail respectively. The mIoUs of these small groups and all categories on the testing set are reported in Table 2. Among the listed methods in Table 2, MinkowskiNet and our Octformer are trained from scratch with random initialization, while CSC-Pretrain [Hou et al. 2021] and SupCon [Khosla et al. 2020] use additional data to pretrain the network with contrastive learning, and LGround [Rozenberszki et al. 2022] is a newly-proposed language-driven pre-training method based on a pretrained large vision-language CLIP model [Radford et al. 2021]. As shown in Table 2, our Octformer trained from scratch without additional data

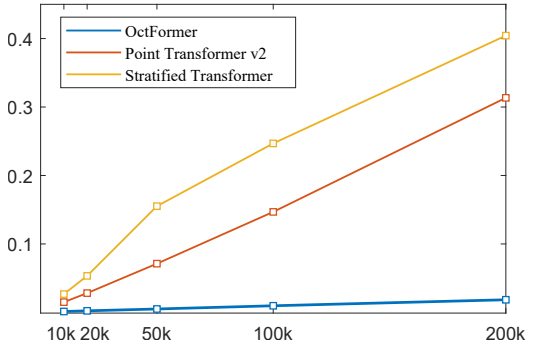


Fig. 4. Efficiency comparisons. The horizontal axis represents the spatial number of an input tensor, and the vertical axis represents the running time in seconds. Our OctFormer runs significantly faster and is over 17 times faster than Point Transformer v2 and Stratified Transformer when the spatial number is 200k.

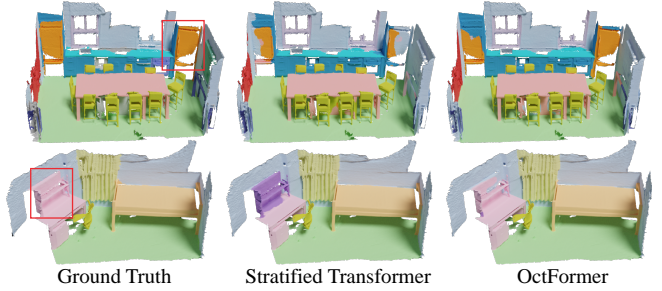


Fig. 5. Visual comparison on ScanNet. The results of OctFormer are more faithful to the ground truth, as highlighted in the rectangle regions.

is significantly better than these competitors and also consistently better in the three small groups, which verifies the effectiveness of our Octformer. Specifically, the mIoU of our OctFormer is higher than MinkowskiNet by 7.3 and higher than LGround by 5.4, although LGround is pretrained with the help of a powerful CLIP model.

## 4.2 Ablation Studies and Discussions

In this section, we justify key design choices of Octformer and compare the efficiency of OctFormer with other point cloud transformers on top of the semantic segmentation on ScanNet in Section 4.1.

*Efficiency.* Global point cloud transformers [Guo et al. 2021; Pang et al. 2022; Yu et al. 2022] can only process point clouds containing several thousand points, thus we omit the comparisons with them and focus on the comparisons with efficient point cloud transformers proposed recently, including Stratified Transformer [Lai et al. 2022] and Point Transformer v2 [Wu et al. 2022]. Stratified Transformer extends window attentions [Liu et al. 2021a] to point clouds with cubic windows [Fan et al. 2022; Sun et al. 2022] and leverages stratified sampling to improve its performance. Point Transformer v2 applies attentions to k nearest neighbors of each point in a sliding-window fashion. Since the network configurations vary greatly, we record the running time of one *single* transformer block on an Nvidia 3090 GPU to eliminate the influence of uncontrolled factors. We choose

Table 3. Ablation studies on semantic segmentation on ScanNet. *mIoU* and *Loss* denote the validation mIoU and the training loss. The training loss is used as a reference of the expressiveness of networks, which is multiplied by 100 for better display. Best results are marked in bold.

(a) Model size. A large model can steadily improve the performance.	(b) Positional encoding. CPE is effective and essential for OctFormer.	(c) Input voxel size. OctFormer is efficient enough to take fine voxels for better results.																																																		
<table border="1"> <thead> <tr> <th>Name</th><th>Model Size</th><th>Loss</th><th>mIoU</th></tr> </thead> <tbody> <tr> <td>Small</td><td>18M</td><td>10.2</td><td>74.0</td></tr> <tr> <td>Base</td><td>39M</td><td>8.12</td><td>74.5</td></tr> <tr> <td>Large</td><td>156M</td><td><b>7.22</b></td><td><b>74.6</b></td></tr> </tbody> </table>	Name	Model Size	Loss	mIoU	Small	18M	10.2	74.0	Base	39M	8.12	74.5	Large	156M	<b>7.22</b>	<b>74.6</b>	<table border="1"> <thead> <tr> <th>Type</th><th>Loss</th><th>mIoU</th></tr> </thead> <tbody> <tr> <td>w/o</td><td>21.7</td><td>66.5</td></tr> <tr> <td>cRPE</td><td>8.43</td><td>73.9</td></tr> <tr> <td>CPE</td><td><b>8.12</b></td><td><b>74.5</b></td></tr> </tbody> </table>	Type	Loss	mIoU	w/o	21.7	66.5	cRPE	8.43	73.9	CPE	<b>8.12</b>	<b>74.5</b>	<table border="1"> <thead> <tr> <th>Voxel Size</th><th>Loss</th><th>mIoU</th></tr> </thead> <tbody> <tr> <td>4cm</td><td>12.6</td><td>70.7</td></tr> <tr> <td>2cm</td><td>9.08</td><td>73.6</td></tr> <tr> <td>1cm</td><td><b>8.12</b></td><td><b>74.5</b></td></tr> </tbody> </table>	Voxel Size	Loss	mIoU	4cm	12.6	70.7	2cm	9.08	73.6	1cm	<b>8.12</b>	<b>74.5</b>										
Name	Model Size	Loss	mIoU																																																	
Small	18M	10.2	74.0																																																	
Base	39M	8.12	74.5																																																	
Large	156M	<b>7.22</b>	<b>74.6</b>																																																	
Type	Loss	mIoU																																																		
w/o	21.7	66.5																																																		
cRPE	8.43	73.9																																																		
CPE	<b>8.12</b>	<b>74.5</b>																																																		
Voxel Size	Loss	mIoU																																																		
4cm	12.6	70.7																																																		
2cm	9.08	73.6																																																		
1cm	<b>8.12</b>	<b>74.5</b>																																																		
(d) Point number in each window. Large point number increases network capacity.	(e) Dilation. Large dilation also increases network capacity.	(f) Data augmentations. Strong data augmentations are helpful for a good mIoU.																																																		
<table border="1"> <thead> <tr> <th>Num.</th><th>Win. Size</th><th>Loss</th><th>mIoU</th></tr> </thead> <tbody> <tr> <td>16</td><td>7</td><td>8.24</td><td>73.8</td></tr> <tr> <td>32</td><td>10</td><td>8.12</td><td><b>74.5</b></td></tr> <tr> <td>48</td><td>12</td><td>8.10</td><td>74.3</td></tr> <tr> <td>64</td><td>15</td><td><b>7.92</b></td><td>74.4</td></tr> </tbody> </table>	Num.	Win. Size	Loss	mIoU	16	7	8.24	73.8	32	10	8.12	<b>74.5</b>	48	12	8.10	74.3	64	15	<b>7.92</b>	74.4	<table border="1"> <thead> <tr> <th>Dilation</th><th>Loss</th><th>mIoU</th></tr> </thead> <tbody> <tr> <td>1</td><td>8.29</td><td>74.2</td></tr> <tr> <td>2</td><td>8.17</td><td>74.4</td></tr> <tr> <td>4</td><td>8.12</td><td><b>74.5</b></td></tr> <tr> <td>8</td><td><b>8.01</b></td><td>74.1</td></tr> </tbody> </table>	Dilation	Loss	mIoU	1	8.29	74.2	2	8.17	74.4	4	8.12	<b>74.5</b>	8	<b>8.01</b>	74.1	<table border="1"> <thead> <tr> <th>Augmentation</th><th>Loss</th><th>mIoU</th></tr> </thead> <tbody> <tr> <td>w/o</td><td><b>0.58</b></td><td>53.8</td></tr> <tr> <td>+Affine</td><td>5.59</td><td>72.7</td></tr> <tr> <td>+Crop</td><td>6.27</td><td>73.6</td></tr> <tr> <td>+Elastic</td><td>8.12</td><td><b>74.5</b></td></tr> </tbody> </table>	Augmentation	Loss	mIoU	w/o	<b>0.58</b>	53.8	+Affine	5.59	72.7	+Crop	6.27	73.6	+Elastic	8.12	<b>74.5</b>
Num.	Win. Size	Loss	mIoU																																																	
16	7	8.24	73.8																																																	
32	10	8.12	<b>74.5</b>																																																	
48	12	8.10	74.3																																																	
64	15	<b>7.92</b>	74.4																																																	
Dilation	Loss	mIoU																																																		
1	8.29	74.2																																																		
2	8.17	74.4																																																		
4	8.12	<b>74.5</b>																																																		
8	<b>8.01</b>	74.1																																																		
Augmentation	Loss	mIoU																																																		
w/o	<b>0.58</b>	53.8																																																		
+Affine	5.59	72.7																																																		
+Crop	6.27	73.6																																																		
+Elastic	8.12	<b>74.5</b>																																																		

the input tensor’s spatial number from  $\{10k, 20k, 50k, 100k, 200k\}$  and set the channel as 96. For the attention modules, we set the head number to 6, and set the point number and neighborhood number to 32 for OctFormer and Point Transformer v2. Since the point number is variant in each window for Stratified Transformer, we set the window size to 6 so that the average point number is about 32.

The results are shown in Figure 4. It can be seen that although the computation complexities of the three methods are all linear, our OctFormer runs significantly faster than Point Transformer v2 and Stratified Transformer. OctFormer runs over 17 times faster than the other two methods when the spatial number of the input tensor is  $200k$ . The key reason for the efficiency of our Octformer is that our novel octree attention mainly leverages standard operators supported by deep learning frameworks, which is further based on general matrix multiplication routines on GPUs and has been optimized towards the computation limit of GPUs. Conversely, the point number in each window of Stratified Transformer is highly unbalanced, making it challenging for efficiency tuning even with hand-crafted GPU programming. Although the neighborhood number of Point Transformer v2 is fixed, the sliding window execution pattern wastes considerable computation that could have been shared.

We also compare the efficiency of the whole network as shown in Figure 1. We record the time of one forward pass of each network on a Nividia 3090 GPU, taking a batch of  $250k$  points. The speed of our Octformer-Small is slightly faster than MinkowskiNet, and faster than Point Transformer V2 by 3 times and Stratified Transformer by 20 times. It is worth mentioning that our OctFormer takes point clouds quantized by a voxel size of 1cm as input, whereas the other networks takes point clouds quantized by a voxel size of 2cm.

**Model Size.** We denote the default OctFormer as OctFormer-Base and design two variants with different amounts of trainable parameters, including OctFormer-Small with half of the parameters of OctFormer-Base and OctFormer-Large with 4 times of parameters of OctFormer-Base. The detailed settings are listed as follows:

- OctFormer-Small:  $C = 96$ , block numbers = {2, 2, 6, 2};
- OctFormer-Large:  $C = 192$ , block numbers = {2, 2, 18, 2}.

We test the performances of these models and summarize the results in Table 3a. It can be seen that as the model size increases, the mIoU on the validation set and the training loss improve steadily. The training loss can be used as a metric that directly reflects the network’s expressiveness. These results indicate that our OctFormer scales up well with increasing model sizes. Note that our OctFormer-Small with only 18M parameters achieves a mIoU of 74.1 (75.2 *with voting*) on the validation set of ScanNet and already surpasses previous sparse-voxel-based CNNs, like Mix3D [Nekrasov et al. 2021] and MinkowskiNet [Choy et al. 2019] with 38M parameters, as shown in Table 1.

**Positional Encoding.** Here we investigate the effect of conditional positional encoding (CPE) [Chu et al. 2021b] and report the results in Table 3b. After removing CPE, denoted as *w/o* in the second row of Table 3b, the mIoU decreases by 8.0, and the training loss also increases greatly, which verifies that the positional encoding is crucial for OctFormer to perceive positional information. Additionally, we also test the contextual relative positional encoding (cRPE) proposed by Stratified Transformer [Lai et al. 2022] with OctFormer and get a mIoU of 73.9, which is much better than the model without positional encoding but still slightly worse than CPE. Although it is possible to further improve the mIoU by tuning the parameters of cRPE, like the quantization size of cRPE, cRPE is tightly coupled with the attention module, and its implementation is more complex than CPE.

**Input Voxel Size.** Octrees are used to rasterize point clouds to sparse voxels, and it is known that finer voxels retain more information, which can help networks achieve better results. We train OctFormer on ScanNet using three different voxel sizes and report the results in Table 3c. OctFormer achieve the best results with a voxel size of 1cm, improving the mIoU by 0.9 compared with a voxel size of 2cm. MinkowskiNet [Choy et al. 2019] and Stratified Transformer [Lai et al. 2022] are typically trained on ScanNet with a voxel size of 2cm by default. However, they run out of memory on Nvidia 3090 GPUs with 24GB memory when using a voxel size of 1cm, requiring further parameter tuning to produce reasonable results. In contrast, our OctFormer, even OctFormer-Large, is efficient enough to be trained with a voxel size of 1cm within 24GB GPU memory.

*Point Number in Each Window.* The point number  $K$  in each window is closely related to the window size and the receptive field of octree attentions. We train OctFormer with a point number chosen from  $\{16, 32, 48, 64\}$  and report the results in Table 3d. With a fixed point number, the window sizes are variable, and we calculated the average window sizes in Table 3d. The window size in Stratified Transformer [Lai et al. 2022] is 5, and the average window size of OctFormer with a default point number of 32 is 10, which greatly increases the receptive field of the network. It is evident from Table 3d that the training loss progressively decreases as the point number increases. Although the mIoU of OctFormer with a point number of 64 is slightly worse than with a point number of 32, the training loss with a point number of 64 is lower, which is a sign of overfitting. Therefore, we can conclude that the expressiveness or capacity of the network increases with the point number of octree attention.

*Dilation.* Dilated octree attentions further increase the receptive field by using dilated local windows, which are controlled by the hyperparameter dilation  $D$ . We train OctFormer with a dilation chosen from  $\{1, 2, 4, 8\}$  and report the results in Table 3e. Similarly, we observe that the mIoU improves until the dilation reaches 4. And the training loss decreases as the dilation increases. When the dilation is 8, the training loss is the best, indicating that the capacity of the network increases with the dilation of octree attention.

*Data Augmentation.* We inspect the influence of different data augmentations on the mIoU by progressively adding each of them and summarize the results in Table 3f. Without data augmentations, we observe severe overfitting, leading to much lower mIoU. As we add more data augmentations, the mIoU gradually increases. Although Mix3D [Nekrasov et al. 2021] leverages an additional 3D mixup augmentation to achieve the best performance on the testing set of ScanNet, we chose to use only the data augmentations in Point Transformer V2 [Wu et al. 2022] and Stratified Transformer [Lai et al. 2022] for a fair comparison with point cloud transformers.

### 4.3 3D Object Detection

In this section, we validate the effectiveness of our OctFormer on 3D object detection. The goal is to predict 3D bounding boxes and the corresponding categories of objects contained in an input point cloud.

*Dataset.* We perform 3D object detection on the SUN RGB-D dataset [Song et al. 2015], which contains about 10k single-view RGB-D scans of indoor scenes. The annotations of RGB-D scans consist of oriented 3D bounding boxes of 37 categories. Following previous settings [Qi et al. 2019; Rukhovich et al. 2022], we use 5285 and 5050 RGB-D scans for training and validation, respectively, and report the average precision (mAP) under IoU thresholds of 0.25 and 0.5, denoted as mAP@0.25 and mAP@0.5, for the ten most common categories for performance comparisons.

*Settings.* We adapt FCAF3D [Rukhovich et al. 2022] with our OctFormer for object detection. FCAF3D currently achieves top performance on the SUN RGB-D detection benchmark. The backbone of FCAF3D is a ResNet with 34 sparse convolution layers built upon MinkowskiNet [Choy et al. 2019]. The detection head of FCAF3D

Table 4. 3D Object detection on SUN RGB-D. The mAP@0.25 and mAP@0.5 denote the mean average precision under IoU threshold of 0.25 and 0.5, respectively. We run the experiments 5 times and report the maximum and average metric values; the average values are shown in brackets. By replacing the backbone of FCAF3D with our OctFormer, we achieve the best performance on mAP@0.5, surpassing all previous state-of-the-art methods.

Method	mAP@0.25	mAP@0.5
VoteNet [Qi et al. 2019]	57.7	-
MLCVNet [Xie et al. 2020]	59.8	-
3DETR [Misra et al. 2021]	59.1	32.7
H3DNet [Zhang et al. 2020b]	60.1	39.0
BRNet [Cheng et al. 2021a]	61.1	43.7
HGNet [Chen et al. 2020]	61.6	-
VENet [Xie et al. 2021]	62.5	39.2
GroupFree [Liu et al. 2021b]	63.0 (62.6)	45.2 (44.4)
CAGroup3D [Wang et al. 2022a]	<b>66.8 (66.4)</b>	50.2 (49.5)
FCAF3D [Rukhovich et al. 2022]	64.2 (63.8)	48.9 (48.2)
OctFormer (ours)	66.2 (65.7)	<b>50.6 (50.2)</b>

is an FPN [Lin et al. 2017], which is widely used in object detection. We replace the original backbone network of FCAF3D with our OctFormer while keeping other components fixed. To be compatible with the configurations of FCAF3D, we further add two octree convolution modules with kernel sizes  $\{3, 2\}$  and stride  $\{1, 2\}$  before the input of OctFormer so that the resolutions of the resulting features are similar to the original backbone of FCAF3D. We perform experiments with the MMDetection3D framework. We employ an AdamW optimizer [Loshchilov and Hutter 2019] to train the network for 18 epochs with a batch size of 32 and a weight decay of 0.01. The initial learning rate is set to 0.001 and decreases by a factor of 10 after 12 and 16 epochs, respectively. The input point clouds are first normalized with a voxel size of 0.01m and then encoded by octrees with a depth of 12, while the initial input features are point colors with 3 channels. The data augmentations include random rotation in  $[-30^\circ, 30^\circ]$  along the upright axis, random scaling in  $[0.85, 1.15]$ , and random translation in  $[-0.1, 0.1]$ , which are similar to FCAF3D.

*Results.* We do comparisons with previous state-of-the-art methods on SUN RGB-D and summarize the results in Table 4. We run our OctFormer 5 times and report the average and maximum performance to reduce the effect of random fluctuations. Each training process takes approximately 3.5 hours on four Nvidia 3090 GPUs, and the maximum GPU memory consumption is less than 8GB. It can be seen from Table 4 that our method achieves the best results in terms of mAP@0.5. Compared with FCAF3D, the only difference is replacing the original backbone of FCAF3D with our OctFormer, and the metrics mAP@0.25 and mAP@0.5 directly increase by 1.9 and 2.0, respectively, which clearly demonstrates the effectiveness of our OctFormer over sparse-voxel-based CNNs. Among the listed methods in Table 4, 3DETR [Misra et al. 2021] and GroupFree [Liu et al. 2021b] are based on point cloud transformers. Our OctFormer achieves significantly better performance than them. Specifically, the mAP@0.25 of our OctFormer is higher than 3DETR and GroupFree by 6.6 and 3.1, and mAP@0.5 is higher by 17.5 and 5.8, respectively. Lastly, it should be noted that the contributions of CAGroup3D [Wang et al.

2022a] are orthogonal to our OctFormer. CAGroup3D mainly improves FCAF3D by designing the detection head, whereas our goal is to demonstrate the advantages of OctFormer over other backbones by replacing the backbone of FCAF3D. Nevertheless, the average mAP@0.5 of our method is still higher than CAGroup3D by 0.7.

## 5 CONCLUSION

We propose OctFormer, a general and effective backbone for 3D point cloud understanding. The core of OctFormer contains a novel octree attention and its dilated variant. Our octree attention is extremely easy to implement and runs significantly faster than other point cloud attentions. OctFormer demonstrates great efficiency and achieves state-of-the-art performance on several benchmarks, including semantic segmentation on ScanNet and ScanNet200 and 3D object detection on SUN RGB-D.

The field of 3D deep learning is rapidly evolving, and it is inevitable that the performance of OctFormer on the leaderboards will be surpassed by future works sooner or later. However, our novel octree attentions, with their highly simplified implementation and super efficiency, along with our unified network design, will make 3D transformers more accessible to a broader audience and open up many exciting possibilities for the future, including pretraining of large-scale general 3D models, cross-modality training with images or languages, and more.

The limitations and future works are discussed as follows:

**Small-Scale Dataset.** One limitation of OctFormer is that it is prone to overfit on small-scale datasets. We test our OctFormer on the ModelNet40 classification, which only contains about 9k shapes for training and 2k for testing. We use the average features produced by the last stage of OctFormer as the shape features for classification and get an accuracy of 92.7% on the testing set without voting. Although OctFormer is superior to the point transformer in Point-BERT [Yu et al. 2022] with an accuracy of 91.2%, it is still worse than PointMLP [Ma et al. 2022] with an accuracy of 94.1%. Point-BERT [Yu et al. 2022] and Point-MAE [Pang et al. 2022] improve the accuracy of their point transformer to 93.8% with unsupervised pre-training. We believe similar unsupervised pretraining techniques can also help OctFormer to combat the overfitting issue to achieve better performance on small-scale datasets, which is left as future work.

**Positional Encoding.** As verified in our ablation studies, positional encoding is essential for transformers, and we currently adopt CPE [Chu et al. 2021b] as the positional encoding of OctFormer. Although CPE is effective, it hurts the flexibility of OctFormer due to the dependency on octree-based depth-wise convolutions. In the future, we will explore the possibility of other positional encodings, e.g., MLP-based positional encoding that encodes the relative positional information with MLPs.

**Cross Attention.** The proposed octree attention is essentially a self-attention, which is mainly used by OctFormer as a building block of an encoder network. Additionally, the cross attention is also indispensable for learning complex relationships between queries and keys and has been successfully used in the decoder of 3DETR [Misra et al. 2021] for 3D object detection. We regard the extension of octree attention to the cross-attention as another future work.

**3D Generation.** We focus on using OctFormer for point cloud understanding tasks in this paper. It is interesting to apply our OctFormer, or other network architectures designed with our octree attention, for 3D content creation with cross-modality training, e.g., 3D shape generation conditioned on images, sketches, or texts.

## ACKNOWLEDGMENTS

This work was supported in part by National Key R&D Program of China 2022ZD0160801. We also thank the anonymous reviewers for their valuable feedback.

## REFERENCES

- Matan Atzmon, Haggai Maron, and Yaron Lipman. 2018. Point Convolutional Neural Networks by Extension Operators. *ACM Trans. Graph. (SIGGRAPH)* 37, 4 (2018).
- Jimmy Lei Ba, Jamie Ryan Kiros, and Geoffrey E Hinton. 2016. Layer normalization. *arXiv preprint arXiv:1607.06450* (2016).
- Jintai Chen, Biwen Lei, Qingyu Song, Haochao Ying, Danny Z Chen, and Jian Wu. 2020. A hierarchical graph network for 3D object detection on point clouds. In *CVPR*.
- Yukang Chen, Jianhui Liu, Xiaojuan Qi, X. Zhang, Jian Sun, and Jiaya Jia. 2022. Scaling up Kernels in 3D CNNs. In *NeurIPS*.
- Bowen Cheng, Lu Sheng, Shaoshuai Shi, Ming Yang, and Dong Xu. 2021a. Back-Tracing Representative Points for Voting-based 3D Object Detection in Point Clouds. In *CVPR*.
- Zhang Cheng, Haocheng Wan, Xinyi Shen, and Zizhao Wu. 2021b. PatchFormer: A versatile 3D transformer based on patch attention. In *CVPR*.
- Hung-Yueh Chiang, Yen-Liang Lin, Yueh-Cheng Liu, and Winston H Hsu. 2019. A unified point-based framework for 3D segmentation. In *3DV*.
- Christopher Choy, Jun Young Gwak, and Silvio Savarese. 2019. 4D spatio-temporal convnets: Minkowski convolutional neural networks. In *CVPR*.
- Xiangxiang Chu, Zhi Tian, Yuqing Wang, Bo Zhang, Haibing Ren, Xiaolin Wei, Huaxia Xia, and Chunhua Shen. 2021a. Twins: Revisiting the Design of Spatial Attention in Vision Transformers. In *NeurIPS*.
- Xiangxiang Chu, Zhi Tian, Bo Zhang, Xinlong Wang, Xiaolin Wei, Huaxia Xia, and Chunhua Shen. 2021b. Conditional positional encodings for vision transformers. *arXiv preprint arXiv:2102.10882* (2021).
- Jean-Baptiste Cordonnier, Andreas Loukas, and Martin Jaggi. 2020. On the relationship between self-attention and convolutional layers. In *ICLR*.
- Angela Dai, Angel X. Chang, Manolis Savva, Maciej Halber, Thomas Funkhouser, and Matthias Nießner. 2017. ScanNet: Richly-annotated 3D Reconstructions of Indoor Scenes. In *CVPR*.
- Angela Dai and Matthias Nießner. 2018. 3DMV: Joint 3D-multi-view prediction for 3D semantic scene segmentation. In *ECCV*.
- Jia Deng, Wei Dong, Richard Socher, Jia Li, Kai Li, and Li Fei-Fei. 2009. ImageNet: A large-scale hierarchical image database. In *CVPR*.
- Xiaoyi Dong, Jianmin Bao, Dongdong Chen, Weiming Zhang, Nenghai Yu, Lu Yuan, Dong Chen, and Baining Guo. 2022. CSWin Transformer: A general vision transformer backbone with cross-shaped windows. In *CVPR*.
- Alexey Dosovitskiy, Lucas Beyer, Alexander Kolesnikov, Dirk Weissenborn, Xiaohua Zhai, Thomas Unterthiner, Mostafa Dehghani, Matthias Minderer, Georg Heigold, Sylvain Gelly, et al. 2021. An image is worth 16x16 words: Transformers for image recognition at scale. In *ICLR*.
- Lue Fan, Ziqi Pang, Tianyuan Zhang, Yu-Xiong Wang, Hang Zhao, Feng Wang, Naiyan Wang, and Zhaoxiang Zhang. 2022. Embracing single stride 3D object detector with sparse transformer. In *CVPR*.
- Matthias Fey, Jan Eric Lenssen, Frank Weichert, and Heinrich Müller. 2018. SplineCNN: Fast Geometric Deep Learning with Continuous B-Spline Kernels. In *CVPR*.
- Benjamin Graham, Martin Engelcke, and Laurens van der Maaten. 2018. 3D semantic segmentation with submanifold sparse convolutional networks. In *CVPR*.
- Meng-Hao Guo, Jun-Xiong Cai, Zheng-Ning Liu, Tai-Jiang Mu, Ralph R Martin, and Shi-Min Hu. 2021. PCT: Point cloud transformer. *Comput. Vis. Media* 7, 2 (2021).
- Ali Hassani and Humphrey Shi. 2022. Dilated neighborhood attention transformer. *arXiv preprint arXiv:2209.15001* (2022).
- Ji Hou, Benjamin Graham, Matthias Nießner, and Saining Xie. 2021. Exploring Data-Efficient 3D Scene Understanding with Contrastive Scene Contexts. In *CVPR*.
- Qingyong Hu, Bo Yang, Linhai Xie, Stefano Rosa, Yulan Guo, Zhihua Wang, Niki Trigoni, and Andrew Markham. 2020a. RandLA-Net: Efficient Semantic Segmentation of Large-Scale Point Clouds. *CVPR*.
- Zeyu Hu, Mingmin Zhen, Xuyang Bai, Hongbo Fu, and Chiew-lan Tai. 2020b. JSENNet: Joint semantic segmentation and edge detection network for 3d point clouds. In *ECCV*.
- Prannay Khosla, Piotr Teterwak, Chen Wang, Aaron Sarna, Yonglong Tian, Phillip Isola, Aaron Maschinot, Ce Liu, and Dilip Krishnan. 2020. Supervised contrastive learning.

- Advances in Neural Information Processing Systems* 33 (2020).
- Alexander Kirillov, Ross Girshick, Kaiming He, and Piotr Dollár. 2019. Panoptic feature pyramid networks. In *CVPR*.
- Xin Lai, Jianhui Liu, Li Jiang, Liwei Wang, Hengshuang Zhao, Shu Liu, Xiaojuan Qi, and Jiaya Jia. 2022. Stratified Transformer for 3D Point Cloud Segmentation. In *CVPR*.
- Huan Lei, Naveed Akhtar, and Ajmal Mian. 2019. Octree guided CNN with spherical kernels for 3D point clouds. In *CVPR*.
- Huan Lei, Naveed Akhtar, and Ajmal Mian. 2020. SegGCN: Efficient 3D point cloud segmentation with fuzzy spherical kernel. In *CVPR*.
- Yangyan Li, Rui Bu, Mingchao Sun, Wei Wu, Xinhua Di, and Baoquan Chen. 2018. PointCNN: Convolution on X-transformed points. In *NeurIPS*.
- Tsung-Yi Lin, Piotr Dollár, Ross Girshick, Kaiming He, Bharath Hariharan, and Serge Belongie. 2017. Feature pyramid networks for object detection. In *CVPR*.
- Ze Liu, Yutong Lin, Yue Cao, Han Hu, Yixuan Wei, Zheng Zhang, Stephen Lin, and Baining Guo. 2021a. Swin transformer: Hierarchical vision transformer using shifted windows. In *ICCV*.
- Ze Liu, Zheng Zhang, Yue Cao, Han Hu, and Xin Tong. 2021b. Group-Free 3D Object Detection via Transformers. In *ICCV*.
- Sergey Loffe and Christian Szegedy. 2015. Batch Normalization: Accelerating deep network training by reducing internal covariate shift. In *ICML*.
- Ilya Loshchilov and Frank Hutter. 2019. Decoupled weight decay regularization. In *ICLR*.
- Xu Ma, Can Qin, Haoxuan You, Haoxi Ran, and Yun Fu. 2022. Rethinking network design and local geometry in point cloud: A simple residual MLP framework. In *ICLR*.
- Jiageng Mao, Yujing Xue, Minzhe Niu, Haoyue Bai, Jiashi Feng, Xiaodan Liang, Hang Xu, and Chunjing Xu. 2021. Voxel Transformer for 3D Object Detection. In *ICCV*.
- Daniel Maturana and Sebastian Scherer. 2015. VoxNet: A 3D convolutional neural network for real-time object recognition. In *IROS*.
- Ishan Misra, Rohit Girdhar, and Armand Joulin. 2021. An End-to-End Transformer Model for 3D Object Detection. In *ICCV*.
- Gaku Narita, Takashi Seno, Tomoya Ishikawa, and Yohsuke Kaji. 2019. PanopticFusion: Online volumetric semantic mapping at the level of stuff and things. In *IROS*.
- Alexey Nekrasov, Jonas Schult, Or Litany, Bastian Leibe, and Francis Engelmann. 2021. Mix3D: Out-of-Context Data Augmentation for 3D Scenes. In *3DV*.
- Yatian Pang, Wenxiao Wang, Francis EH Tay, Wei Liu, Yonghong Tian, and Li Yuan. 2022. Masked autoencoders for point cloud self-supervised learning. In *ECCV*.
- Chunghyun Park, Yoonwoo Jeong, Minsu Cho, and Jaesik Park. 2022. Fast Point Transformer. In *CVPR*.
- Adam Paszke, Sam Gross, Francisco Massa, Adam Lerer, James Bradbury, Gregory Chanan, Trevor Killeen, Zeming Lin, Natalia Gimelshein, Luca Antiga, Alban Desimone, Andreas Kopf, Edward Yang, Zachary DeVito, Martin Raison, Alykhan Tejani, Sasank Chilamkurthy, Benoit Steiner, Lu Fang, Junjie Bai, and Soumith Chintala. 2019. PyTorch: An Imperative Style, High-Performance Deep Learning Library. In *NeurIPS*.
- Charles R. Qi, Or Litany, Kaiming He, and Leonidas J. Guibas. 2019. Deep Hough Voting for 3D Object Detection in Point Clouds. In *CVPR*.
- Charles R. Qi, Hao Su, Kaichun Mo, and Leonidas J. Guibas. 2017a. PointNet: Deep learning on point sets for 3D classification and segmentation. In *CVPR*.
- Charles R. Qi, Hao Su, Matthias Nießner, Angela Dai, Mengyuan Yan, and Leonidas J. Guibas. 2016. Volumetric and multi-view CNNs for object classification on 3D data. In *CVPR*.
- Charles R. Qi, Li Yi, Hao Su, and Leonidas J. Guibas. 2017b. PointNet++: Deep hierarchical feature learning on point sets in a metric space. In *NeurIPS*.
- Alec Radford, Jong Wook Kim, Chris Hallacy, Aditya Ramesh, Gabriel Goh, Sandhini Agarwal, Girish Sastry, Amanda Askell, Pamela Mishkin, Jack Clark, et al. 2021. Learning transferable visual models from natural language supervision. In *ICML*.
- Colin Raffel, Noam Shazeer, Adam Roberts, Katherine Lee, Sharan Narang, Michael Matena, Yanqi Zhou, Wei Li, Peter J Liu, et al. 2020. Exploring the limits of transfer learning with a unified text-to-text transformer. *J. Mach. Learn. Res.* 21, 140 (2020).
- Aditya Ramesh, Prafulla Dhariwal, Alex Nichol, Casey Chu, and Mark Chen. 2022. Hierarchical text-conditional image generation with CLIP latents. *arXiv preprint arXiv:2204.06125* (2022).
- Gernot Riegler, Ali Osman Ulusoy, Horst Bischof, and Andreas Geiger. 2017b. OctNet-Fusion: Learning depth fusion from data. In *3DV*.
- Gernot Riegler, Ali Osman Ulusoy, and Andreas Geiger. 2017a. OctNet: Learning deep 3D representations at high resolutions. In *CVPR*.
- David Rozenberszki, Or Litany, and Angela Dai. 2022. Language-Grounded Indoor 3D Semantic Segmentation in the Wild. In *ECCV*.
- Danila Rukhovich, Anna Vorontsova, and Anton Konushin. 2022. FCAF3D: fully convolutional anchor-free 3D object detection. In *ECCV*.
- Tianjia Shao, Yin Yang, Yanlin Weng, Qiming Hou, and Kun Zhou. 2018. H-CNN: spatial hashing based CNN for 3D shape analysis. *IEEE. T. Vis. Comput. Gr.* (2018).
- Martin Simonovsky and Nikos Komodakis. 2017. Dynamic edge-conditioned filters in convolutional neural networks on graphs. In *CVPR*.
- Shuran Song, Samuel P Lichtenberg, and Jianxiong Xiao. 2015. SUN RGB-D: A RGB-D scene understanding benchmark suite. In *CVPR*.
- Hang Su, Subhransu Maji, Evangelos Kalogerakis, and Erik Learned-Miller. 2015. Multi-view convolutional neural networks for 3D shape recognition. In *ICCV*.
- Pei Sun, Mingxing Tan, Weiyu Wang, Chenxi Liu, Fei Xia, Zhaoqi Leng, and Dragomir Anguelov. 2022. SWFormer: Sparse Window Transformer for 3D Object Detection in Point Clouds. In *ECCV*.
- Hugues Thomas, Charles R. Qi, Jean-Emmanuel Deschaud, Beatriz Marcotegui, François Goulette, and Leonidas J. Guibas. 2019. KPConv: Flexible and deformable convolution for point clouds. In *ICCV*.
- Zhengzhong Tu, Hossein Talebi, Han Zhang, Feng Yang, Peyman Milanfar, Alan Bovik, and Yinxiao Li. 2022. MaxViT: Multi-Axis Vision Transformer. In *ECCV*.
- Ashish Vaswani, Noam Shazeer, Niki Parmar, Jakob Uszkoreit, Llion Jones, Aidan N Gomez, Łukasz Kaiser, and Illia Polosukhin. 2017. Attention is all you need. In *NeurIPS*.
- Haiyang Wang, Lihe Ding, Shaocong Dong, Shaoshuai Shi, Aoxue Li, Jianan Li, Zhen-guo Li, and Liwei Wang. 2022a. CAGroup3D: Class-aware grouping for 3D object detection on point clouds. In *NeurIPS*.
- Peng-Shuai Wang, Yang Liu, Yu-Xiao Guo, Chun-Yu Sun, and Xin Tong. 2017. O-CNN: Octree-based convolutional neural networks for 3D shape analysis. *ACM Trans. Graph. (SIGGRAPH)* 36, 4 (2017).
- Peng-Shuai Wang, Chun-Yu Sun, Yang Liu, and Xin Tong. 2018. Adaptive O-CNN: A patch-based deep representation of 3D shapes. *ACM Trans. Graph. (SIGGRAPH ASIA)* 37, 6 (2018).
- Wenhai Wang, Enze Xie, Xiang Li, Deng-Ping Fan, Kaitao Song, Ding Liang, Tong Lu, Ping Luo, and Ling Shao. 2021. Pyramid vision transformer: A versatile backbone for dense prediction without convolutions. In *ICCV*.
- Wenhai Wang, Enze Xie, Xiang Li, Deng-Ping Fan, Kaitao Song, Ding Liang, Tong Lu, Ping Luo, and Ling Shao. 2022b. PVT v2: Improved baselines with pyramid vision transformer. *Comput. Vis. Media* 8, 3 (2022).
- Ross Wightman. 2019. PyTorch Image Models. <https://github.com/rwightman/pytorch-image-models>.
- Jane Wilhelms and Allen Van Gelder. 1992. Octrees for faster isosurface generation. *ACM Trans. Graph.* 11, 3 (1992).
- Wenxuan Wu, Zhongang Qi, and Li Fuxin. 2019. PointConv: Deep Convolutional Networks on 3D Point Clouds. In *CVPR*.
- Xiaoyang Wu, Yixing Lao, Li Jiang, Xihui Liu, and Hengshuang Zhao. 2022. Point Transformer V2: Grouped Vector Attention and Partition-based Pooling. In *NeurIPS*.
- Zhirong Wu, Shuran Song, Aditya Khosla, Fisher Yu, Linguang Zhang, Xiaozou Tang, and Jianxiong Xiao. 2015. 3D ShapeNets: A deep representation for volumetric shape modeling. In *CVPR*.
- Tete Xiao, Mannat Singh, Eric Mintun, Trevor Darrell, Piotr Dollár, and Ross Girshick. 2021. Early convolutions help transformers see better. In *NeurIPS*.
- Qian Xie, Yu-Kun Lai, Jing Wu, Zhoutao Wang, Dening Lu, Mingqiang Wei, and Jun Wang. 2021. VENet: Voting Enhancement Network for 3D Object Detection. In *ICCV*.
- Qian Xie, Yu-Kun Lai, Jing Wu, Zhoutao Wang, Yiming Zhang, Kai Xu, and Jun Wang. 2020. MLCVNet: Multi-level context votenet for 3D object detection. In *CVPR*.
- Yifan Xu, Tianqi Fan, Mingye Xu, Long Zeng, and Yu Qiao. 2018. SpiderCNN: Deep Learning on Point Sets with Parameterized Convolutional Filters. In *ECCV*.
- Xu Yan, Chaoda Zheng, Zhen Li, Sheng Wang, and Shuguang Cui. 2020. PointASNL: Robust point clouds processing using nonlocal neural networks with adaptive sampling. In *CVPR*.
- Jianwei Yang, Chunyu Li, Pengchuan Zhang, Xiyang Dai, Bin Xiao, Lu Yuan, and Jianfeng Gao. 2021. Focal Self-attention for Local-Global Interactions in Vision Transformers. In *NeurIPS*.
- Xumin Yu, Lulu Tang, Yongming Rao, Tiejun Huang, Jie Zhou, and Jiwen Lu. 2022. Point-BERT: Pre-training 3D point cloud transformers with masked point modeling. In *CVPR*.
- Feihu Zhang, Jin Fang, Benjamin Wah, and Philip Torr. 2020a. Deep FusionNet for point cloud semantic segmentation. In *ECCV*.
- Zaiwei Zhang, Bo Sun, Haitao Yang, and Qixing Huang. 2020b. H3DNet: 3D object detection using hybrid geometric primitives. In *ECCV*.
- Hengshuang Zhao, Li Jiang, Jiaya Jia, Philip Torr, and Vladlen Koltun. 2021. Point transformer. In *ICCV*.
- Kun Zhou, Minmin Gong, Xin Huang, and Baining Guo. 2011. Data-parallel octrees for surface reconstruction. *IEEE. T. Vis. Comput. Gr.* 17, 5 (2011).

Received January 2023; accepted March 2023; final version May 2023